Journal of Solid Mechanics Vol. 7, No. 2 (2015) pp. 131-145

Semi Analytical Analysis of FGM Thick-Walled Cylindrical Pressure Vessel with Longitudinal Variation of Elastic Modulus under Internal Pressure

M. Shariati [1], H. Sadeghi [2], M. Ghannad [2],H. Gharooni [2,*]

[1]*Department of Mechanical Engineering, Ferdosi University, Mashhad, Iran*
[2]*Department of Mechanical Engineering, Shahrood University, Shahrood, Iran*

Received 15 February 2015; accepted 3 April 2015

ABSTRACT

In this paper, a numerical analysis of stresses and displacements in FGM thick-walled cylindrical pressure vessel under internal pressure has been presented. The elastic modulus is assumed to be varying along the longitude of the pressure vessel with an exponential function continuously. The Poisson's ratio is assumed to be constant. Whereas most of the previous studies about FGM thick-walled pressure vessels are on the basis of changing material properties along the radial direction, in this research, elastic analysis of cylindrical pressure vessel with exponential variations of elastic modulus along the longitudinal direction, under internal pressure, have been investigated. For the analysis of the vessel, the stiffness matrix of the cylindrical pressure vessel has been extracted by the usage of Galerkin Method and the numerical solution for axisymmetric cylindrical pressure vessel under internal pressure have been presented. Following that, displacements and stress distributions depending on inhomogeneity constant of FGM vessel along the longitudinal direction of elastic modulus, are illustrated and compared with those of the homogeneous case. The values which have been used in this study are arbitrary chosen to demonstrate the effect of inhomogeneity on displacements and stress distributions. Finally, the results are compared with the findings of finite element method (FEM).
© 2015 IAU, Arak Branch.All rights reserved.

Keywords : Thick-walled cylinder; Cylindrical pressure vessel; FGM; Longitudinal variations of elastic modulus; Exponential.

1 INTRODUCTION

BECAUSE of good thermal and mechanical properties, the layered composites have been used widely in different branches of engineering. The main defect of these materials is rapid change in common limit of their layers that results stress concentration and undesirable effects. Although the functionally graded materials (FGM) have the mechanical and thermal properties of layered composites, they have not mentioned problem. The remarkable characteristics of these materials are for their composite essence and the changes of material properties gradually at common limit that result decrease of both residual stresses and concentration of stresses and increase the mechanical stresses bearing. Cylindrical shells are common structural elements in many engineering applications. For instance in exteriors of rockets and missiles or pressure vessels, the existence of pressure gradient along the longitudinal direction of the cylinder make the engineers to use cylindrical shell with variable thickness.

*Corresponding author. Tel.: +98 9153056995.
E-mail address: gharooni.hamed@gmail.com (H.Gharooni).

© 2015 IAU, Arak Branch. All rights reserved.

Nowadays, thick-walled cylindrical shells with constant thickness made of functionally graded material are used instead of homogenous cylinders with variable thickness. Besides limitation of designing and production processes of variable-thickness cylinders, it was shown that the mechanical properties of FG cylinders with varying material properties along the longitudinal direction were greatly improved in comparison with that of the common homogenous ones in mentioned structures. Furthermore, idea of FGM theory was used to the design of gradient ceramic nozzle. The purpose was to increase the erosion wear resistance at the entrance of the nozzle by the usage of varying mechanical properties of the constituent layers along the longitudinal direction in these laminated materials.

Fukui and Yamanaka used the Navier solution for derivation of the governing equation of a thick-walled FGM tube under internal pressure and solved the obtained equation numerically by means of the Runge-Kutta method [1]. Tutuncu and Ozturk obtained the closed-form solutions for stresses and displacements in Functionally Graded cylindrical and spherical shells subjected to internal pressure with assumption of elastic modulus changes along the radial direction with exponential function [2]. Jabbari and Eslami presented solution of a FGM cylindrical vessel, under thermal and mechanical loading symmetrically [3]. Eipakchi et. al. have investigated homogenous and isotropic conical shells with variable thickness using FSDT and SSDT (second-order shear deformation theory) and solve the conducted equations by perturbation theory [4]. Eslami and Babaei analyzed FGM thick-walled sphere under the effect of mechanical and thermal stresses [5]. Dai and Fu obtained closed-form solution of FGM pressure vessels under the effect of uniform magnetic field [6]. Naghdabadi and Kordkheili formulated FGM plates and shells with changes of material properties along the radial direction using finite element method [7]. Hongjun et al. indicated the exact solution of FGM hollow cylinders in the state of plane strain with exponential function of elasticity modulus along the radius [8]. Zhifei et al. analyzed heterogeneous cylindrical shells with power function of elasticity modulus by the usage of multilayer method with homogeneous layers [9]. Thick-walled FGM cylinders in plane strain state with exponentially-varying material properties were solved by Tutuncu using Frobenius method [10]. Ghannad et al. present the general method of derivation and the analysis of internally pressurized thick-walled cylinders with clamped-clamped ends [11]. Ghannad et al. presented a closed form analytical solution for clamped-clamped thick cylindrical shells with variable thickness subjected to constant internal pressure based on the first-order shear deformation theory (FSDT) [12]. Gharooni and Ghannad investigate the general solution of rotating FGM pressurized thick hollow cylinder with exponentially varying properties under clamped-clamped conditions based on FSDT [13].

Deng et al. indicated a model for the design of gradient ceramic nozzle materials by the purpose of reducing the tensile stress at the entry region of the nozzle during sand blasting processes [14]. Liu and Deng investigated the erosion behavior of the gradient ceramic nozzles in comparison with the common homologous ceramic nozzles [15]. The experimental and FEM results have shown that the ceramic nozzles with a gradient structure have superior erosion wear resistance and the surface Vickers hardness and indentation fracture toughness of gradient ceramic nozzle were greatly improved compared with that of the common homologous ones. Asgari and Akhlaghi considered transient thermal stresses in a thick hollow cylinder with finite length made of two-dimensional functionally graded material (2D-FGM) based on classical theory of thermoelasticity [16]. The volume fraction distribution of materials, geometry and thermal load are assumed to be axisymmetric but not uniform along the axial direction. Also the effects of material distribution in two radial and axial directions on the thermal stress distribution and time responses are studied. Asemi et al. studied a thick truncated hollow cone with finite length made of two-dimensional functionally graded materials (2D-FGM) subjected to combined loads. The volume fraction distribution of materials and geometry are assumed to be axisymmetric but not uniform along the axial direction [17]. Ghannad et al. presented an analytical solution for deformations and stresses of axisymmetric clamped–clamped thick cylindrical shells with variable thickness made of functionally graded materials (FGMs) subjected to internal pressure by the usage of the first-order shear deformation theory (FSDT) and matched asymptotic method (MAM) of the perturbation theory [18]. The modulus of elasticity distribution was assumed to be the function of radial and longitudinal direction.

It is obviously observed that most of the previous researches on FGM thick-walled cylinders and pressure vessels have been done on the FG materials with variation of material properties along the radial direction. Furthermore, scarce recent studies on FG cylinders with longitudinal variation of material properties are limited to finite element modeling of laminated ones. It was shown that using FG cylinders with varying material properties along the longitudinal direction improve mechanical properties and are suitable substitute for homogeneous cylinders with variable thickness in industries, especially in cases where pressure gradient along the longitudinal direction of the cylinder exist. In this article , therefore, a numerical method for elastic analysis of an internally pressurized thick-walled cylindrical pressure vessels made of functionally graded material with constant Poisson's ratio and exponentially varying elastic modulus along the longitudinal direction have been presented. The stiffness

© 2015 IAU, Arak Branch

matrix of the cylindrical pressure vessel has been extracted by the usage of Galerkin Method. Finally, the results are compared with the findings of finite element method.

2 EXTRACTING STIFFNESS MATRICES OF FG CYLINDRICAL PRESSURE VESSEL

In this section, by the usage of equilibrium equations and Galerkin Method, the stiffness matrix of FGM thick-walled cylindrical pressure vessel with exponential variation of elastic modulus along longitudinal direction has been extracted. The parameter r is the radius of each layer of pressure vessel and z is the length variable (see Fig. 1):

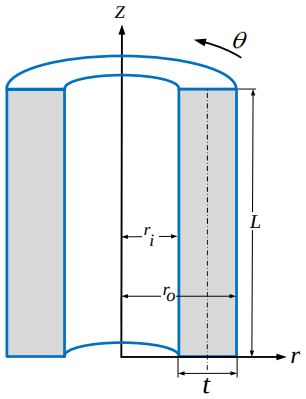

Fig.1
Geometry of the thick pressure vessel.

Parameters t and L are the thickness and the length of the cylinder, respectively. For the axisymmetric conditions, the equilibrium equations are:

$$\left\{\frac{\partial}{\partial r}\sigma_r+\frac{\partial}{\partial z}\tau_{rz}+\frac{\sigma_r-\sigma_\theta}{r}=0\right. \tag{1}$$

$$\left\{\frac{\partial}{\partial r}\tau_{rz}+\frac{\partial}{\partial z}\sigma_z+\frac{\tau_{rz}}{r}=0\right. \tag{2}$$

By the usage of Galerkin Method, Eq. (1) varies as follows;

$$\iint\left(\frac{\partial}{\partial r}\sigma_r+\frac{\partial}{\partial z}\tau_{rz}+\frac{\sigma_r-\sigma_\theta}{r}\right)\phi_i r dr dz=0 \tag{3}$$

We have:

$$\iint\left(\frac{\partial}{\partial r}\left(r\phi_i\sigma_r\right)-\phi_i\sigma_r-\frac{\partial\phi_i}{\partial r}r\sigma_r-\frac{\partial}{\partial z}\left(-\phi_i r\tau_{rz}\right)-\frac{\partial\phi_i}{\partial z}r\tau_{rz}+\sigma_r\phi_i-\sigma_\theta\phi_i\right)dr dz=0 \tag{4}$$

On the basis of Green Theorem, we have:

$$\iint\left(\frac{\partial M}{\partial r}-\frac{\partial Q}{\partial z}\right)dr\ dz=\int_c Q\ dr+\int_c M\ dz \tag{5}$$

Applying Eq. (5) to Eq. (4) resulted:

$$\iint\phi_i\sigma_r dr dz+\iint\frac{\partial\phi_i}{\partial r}r\sigma_r dr dz+\iint\frac{\partial\phi_i}{\partial z}r\tau_{rz}dr dz-\iint\phi_i\sigma_r dr dz+\iint\phi_i\sigma_\theta dr dz=\int-\phi_i r\tau_{rz}dr+\int r\phi_i\sigma_r dz \tag{6}$$

© 2015 IAU, Arak Branch

The mechanical kinematic relations in the cylindrical coordinates system for an axisymmetric cylinder are:

$$\begin{cases} \varepsilon_r = \dfrac{\partial u}{\partial r} \\ \varepsilon_\theta = \dfrac{u}{r} \\ \varepsilon_z = \dfrac{\partial w}{\partial z} \\ \gamma_{rz} = \dfrac{\partial u}{\partial z} + \dfrac{\partial w}{\partial r} \end{cases} \tag{7}$$

where u and w are radial and axial components of displacement field respectively.

Modulus of elasticity E is supposed to be an exponential function of longitudinal direction and assumed to vary as follows:

$$E(z) = E_0 e^{z\beta} \tag{8}$$

where E_0 is the modulus of elasticity at the end boundary (clamped condition) of pressure vessel $(z=0)$ and β is the FG material inhomogeneity constant which have been determined empirically. Fig. 2 shows the distribution of normalized elasticity modulus with respect to the normalized length in a heterogeneous cylinder for integer values of β.

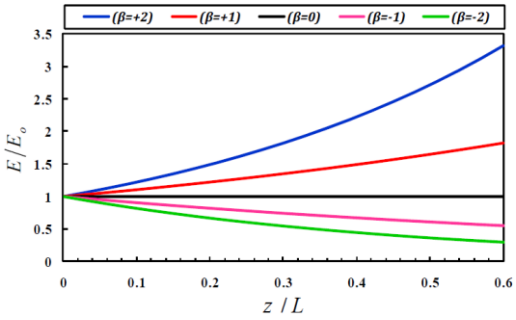

Fig.2
Distribution of normalized elasticity modulus in FGM cylinder.

On the basis of the constitutive equations for inhomogeneous and isotropic materials, the stress-strain relations are as follows:

$$\begin{cases} \sigma_r = C_{11}\varepsilon_r + C_{12}\varepsilon_z + C_{13}\gamma_{rz} + C_{14}\varepsilon_\theta \\ \sigma_z = C_{21}\varepsilon_r + C_{22}\varepsilon_z + C_{23}\gamma_{rz} + C_{24}\varepsilon_\theta \\ \tau_{rz} = C_{31}\varepsilon_r + C_{32}\varepsilon_z + C_{33}\gamma_{rz} + C_{34}\varepsilon_\theta \\ \sigma_\theta = C_{41}\varepsilon_r + C_{42}\varepsilon_z + C_{43}\gamma_{rz} + C_{44}\varepsilon_\theta \end{cases} \tag{9}$$

Considering elasticity modulus variation based on Eq. (8), the stiffness matrices of stress-strain relation for axisymmetric condition have been conducted.

$$[C] = \frac{E_0 e^{z\beta}}{(1+\nu)(1-2\nu)} \begin{bmatrix} 1-\nu & \nu & 0 & \nu \\ \nu & 1-\nu & 0 & \nu \\ 0 & 0 & \dfrac{1-2\nu}{2} & 0 \\ \nu & \nu & 0 & 1-\nu \end{bmatrix} \tag{10}$$

Using triangular elements in numerical solution of cylinder yields to:

© 2015 IAU, Arak Branch

$$\begin{cases} u = \sum a_j \ \phi_j \\ w = \sum b_j \ \phi_j \\ \phi_i = C_i r + D_i z + E_i \\ \phi_j = C_j r + D_j z + E_j \end{cases} \qquad i, j = 1,2,3 \tag{11}$$

where r_i and z_i are the radial and longitudinal coordinates of triangular element nodes respectively. Furthermore, C_i, D_i and E_i are as follows:

$$\begin{Bmatrix} C_1 \\ D_1 \\ E_1 \end{Bmatrix} = g^{-1} \begin{Bmatrix} 1 \\ 0 \\ 0 \end{Bmatrix} \tag{12a}$$

$$\begin{Bmatrix} C_2 \\ D_2 \\ E_2 \end{Bmatrix} = g^{-1} \begin{Bmatrix} 0 \\ 1 \\ 0 \end{Bmatrix} \tag{12b}$$

$$\begin{Bmatrix} C_3 \\ D_3 \\ E_3 \end{Bmatrix} = g^{-1} \begin{Bmatrix} 0 \\ 0 \\ 1 \end{Bmatrix} \tag{12c}$$

where $[g]$ is

$$[g] = \begin{bmatrix} r_1 & z_1 & 1 \\ r_2 & z_2 & 1 \\ r_3 & z_3 & 1 \end{bmatrix} \tag{13}$$

Using Eqs. (6) - (13), we have:

$$\begin{aligned} &\sum a_j \left[\iint C_i r \left(C_{11} C_j + C_{13} C_j \right) + C_i r C_{14} \frac{\phi_j}{r} + D_i r \left(C_{31} C_j + C_{33} D_j \right) + D_i r C_{34} \frac{\phi_j}{r} \left(C_{41} C_j + C_{43} D_j \right) \right. \\ &\left. + C_{44} \phi_j \frac{\phi_j}{r} \right] dr dz + \sum b_j \left[\iint C_i r \left(C_{12} C_j + C_{13} C_j \right) + D_i r \left(C_{32} C_j + C_{33} D_j \right) - \phi_i \left(-C_{42} D_j - C_{43} C_j \right) \right] dr dz \\ &= \int -\phi_i r \tau_{rz} dr + \int \phi_i r \sigma_r dz \end{aligned} \tag{14}$$

Considering very small triangular elements, the right hand side of Eq. (14) varies as follows by appropriate approximation.

$$\begin{aligned} &\sum a_j A_e \left[C_i r \left(C_{11} C_j + C_{13} D_j + C_{14} \frac{\phi_j}{r} \right) + D_i r \left(C_{31} C_j + C_{33} D_j + C_{34} \frac{\phi_j}{r} \right) + \phi_i \left(C_{41} C_j + C_{43} D_j + C_{44} \frac{\phi_j}{r} \right) \right]_{z=\bar{z}}^{r=\bar{r}} \\ &+ \sum b_j A_e \left[C_i r \left(C_{12} D_j + C_{13} C_j \right) + D_i r \left(C_{32} D_j + C_{33} C_j \right) + \phi_i \left(C_{42} D_j + C_{43} C_j \right) \right]_{z=\bar{z}}^{r=\bar{r}} \end{aligned} \tag{15}$$

where $\bar{r}$ and $\bar{z}$ are the radial and longitudinal coordinates at the center of element, respectively and A_e represent the area of element.

$$\bar{r} = \frac{r_1 + r_2 + r_3}{3} \tag{16a}$$

© 2015 IAU, Arak Branch

$$\bar{z} = \frac{z_1 + z_2 + z_3}{3} \tag{16b}$$

$$A_e = \frac{1}{2}\begin{vmatrix} r_1 & z_1 & 1 \\ r_2 & z_2 & 1 \\ r_3 & z_3 & 1 \end{vmatrix} \tag{16c}$$

The similar derivation, as Eq. (1), has been used for Eq. (2). By the usage of Galerkin method, Eq. (2) is converted as follow:

$$\int\left(\frac{\partial}{\partial r}\tau_{rz} + \frac{\partial}{\partial z}\sigma_z + \frac{\tau_{rz}}{r}\right)\phi_i r dr dz = \iint\left[\frac{\partial}{\partial r}\left(\tau_{rz} r\phi_i\right) - \frac{\partial\phi_i}{\partial r} r\tau_{rz} - \tau_{rz}\phi_i - \frac{\partial}{\partial z}\left(-\sigma_z\phi_i r\right) - \frac{\partial\phi_i}{\partial z}\sigma_z r + \tau_{rz}\phi_i\right] dr dz = 0 \tag{17}$$

Eq. (17) could be simplified as follow:

$$\int -\sigma_z\phi_i r dr + \int \tau_{rz} r\phi_i dz - \iint \frac{\partial\phi_i}{\partial r} r\tau_{rz} dr dz - \iint \tau_{rz}\phi_i dr dz - \iint \frac{\partial\phi_i}{\partial z}\sigma_z r dr dz + \iint \tau_{rz}\phi_i dr dz = 0 \tag{18}$$

Using Eqs. (5) and (18), yields:

$$\iint \frac{\partial\phi_i}{\partial r} r\tau_{rz} dr dz + \iint \frac{\partial\phi_i}{\partial z}\sigma_z r dr dz = -\int \sigma_z\phi_i r dr + \int \tau_{rz} r\phi_i dz \tag{19}$$

By the usage of Eqs. (7) to (13), Eq. (19) becomes:

$$\begin{aligned} &\sum a_j \left[\iint C_i r\left(C_{31}C_j + C_{33}D_j + C_{34}\frac{\phi_j}{r}\right) + D_i r\left(C_{21}C_j + C_{23}D_j + C_{24}\frac{\phi_j}{r}\right)\right] dr dz \\ &+\sum b_j \left[\iint C_i r\left(C_{32}D_j + C_{33}C_j\right) + D_i r\left(C_{22}D_j + C_{23}C_j\right)\right] dr dz = -\int \sigma_z\phi_i r dr + \int \tau_{rz} r\phi_i dz \end{aligned} \tag{20}$$

Considering very small triangular elements, Eq. (20) by the usage of Eq. (16) and appropriate approximation yields:

$$\begin{aligned} &\sum a_j A_e \left[C_i r\left(C_{31}C_j + C_{33}D_j + C_{34}\frac{\phi_j}{r}\right) + D_i r\left(C_{21}C_j + C_{23}D_j + C_{24}\frac{\phi_j}{r}\right)\right]_{z=\bar{z}}^{r=\bar{r}} \\ &+\sum b_j A_e \left[C_i r\left(C_{32}D_j + C_{33}C_j\right) + D_j r\left(C_{22}D_j + C_{23}C_j\right)\right]_{z=\bar{z}}^{r=\bar{r}} = \int -\sigma_z\phi_i r dr + \int \tau_{rz} r\phi_i dz \end{aligned} \tag{21}$$

The elements of stiffness matrices for FGM thick-walled cylindrical pressure vessel could be obtained. Stiffness matrices have 36 members (6×6), which have been resulted from left hand side of indicial Eqs. (15) and (21). Each of these two equations for *i*=1, 2 and 3 generate three equations and finally have been converted to six equations. From indicial Eq. (15), for *i*=1, 2 and 3, the elements of first, third and fifth lines, and from indicial Eq. (21), for *i*=1, 2 and 3, the elements of second, fourth and six lines of the element stiffness matrices would be resulted, respectively.

Considering a_j and b_j as the radial and axial displacements of triangular element's nodes named "*j*", respectively, in the left hand side of three expanded equations resulted from indicial Eq. (15), whatever is defined as the displacement's coefficient of a_j (for *j*=1, 2 and 3) are the odd elements of odd lines in stiffness matrices and whatever is defined as the coefficient of b_j (for *j*=1, 2 and 3) are the even elements of odd lines in stiffness matrices. Furthermore, in the left hand side of three equations resulted from Eq. (21), whatever defined as the coefficient of a_j (for *j*=1, 2 and 3) are the odd elements of even lines in stiffness matrices, and whatever defined as the coefficient of b_j (for j=1, 2 and 3) are the even elements of even lines in stiffness matrices, respectively. For instance,

© 2015 IAU, Arak Branch

construction of the elements in the first line of stiffness matrices, for *j*=1, 2, 3 and *i*=1, in Eqs. (15) and (21) have been shown in Eqs. (22) and (23).

$$a_1K_{11}+a_2K_{13}+a_3K_{15}+b_1K_{12}+b_2K_{14}+b_3K_{16}=-\int\tau_{rz}\phi_1 rdr+\int\sigma_r\phi_1 rdz \tag{22}$$

$$a_1K_{21}+a_2K_{23}+a_3K_{25}+b_1K_{22}+b_2K_{24}+b_3K_{26}=-\int\sigma_z\phi_1 rdr+\int\tau_{rz}\phi_1 rdz \tag{23}$$

where K_{1i} and K_{2i} are as follows:

$$K_{11}=A_e\left[C_1r\left(C_{11}C_1+C_{13}D_1+C_{14}\frac{\varphi_1}{r}\right)+D_1r\left(C_{31}C_1+C_{33}D_1+C_{34}\frac{\varphi_1}{r}\right)+\varphi_1\left(C_{41}C_1+C_{43}D_1+C_{44}\frac{\varphi_1}{r}\right)\right] \tag{24a}$$

$$K_{13}=A_e\left[C_1r\left(C_{11}C_2+C_{13}D_2+C_{14}\frac{\varphi_2}{r}\right)+D_1r\left(C_{31}C_2+C_{33}D_2+C_{34}\frac{\varphi_2}{r}\right)+\varphi_1\left(C_{41}C_2+C_{43}D_2+C_{44}\frac{\varphi_2}{r}\right)\right] \tag{24b}$$

$$K_{15}=A_e\left[C_1r\left(C_{11}C_3+C_{13}D_3+C_{14}\frac{\varphi_3}{r}\right)+D_1r\left(C_{31}C_3+C_{33}D_3+C_{34}\frac{\varphi_3}{r}\right)+\varphi_1\left(C_{41}C_3+C_{43}D_3+C_{44}\frac{\varphi_3}{r}\right)\right] \tag{24c}$$

$$K_{12}=A_e\left[C_1r\left(C_{12}D_1+C_{13}C_1\right)+D_1r\left(C_{32}D_1+C_{33}C_1\right)+\varphi_1\left(C_{42}D_1+C_{43}C_1\right)\right] \tag{24d}$$

$$K_{14}=A_e\left[C_1r\left(C_{12}D_2+C_{13}C_2\right)+D_1r\left(C_{32}D_2+C_{33}C_2\right)+\varphi_1\left(C_{42}D_2+C_{43}C_2\right)\right] \tag{24e}$$

$$K_{16}=A_e\left[C_1r\left(C_{12}D_3+C_{13}C_3\right)+D_1r\left(C_{32}D_3+C_{33}C_3\right)+\varphi_1\left(C_{42}D_3+C_{43}C_3\right)\right] \tag{24f}$$

$$K_{21}=A_e\left[C_1r\left(C_{31}C_1+C_{33}D_2+C_{34}\frac{\varphi_1}{r}\right)+D_1r\left(C_{21}C_1+C_{23}D_1+C_{24}\frac{\varphi_1}{r}\right)\right] \tag{25a}$$

$$K_{23}=A_e\left[C_1r\left(C_{31}C_2+C_{33}D_2+C_{34}\frac{\varphi_2}{r}\right)+D_1r\left(C_{21}C_2+C_{23}D_2+C_{24}\frac{\varphi_2}{r}\right)\right] \tag{25b}$$

$$K_{25}=A_e\left[C_1r\left(C_{31}C_3+C_{33}D_3+C_{34}\frac{\varphi_3}{r}\right)+D_1r\left(C_{21}C_3+C_{23}D_3+C_{24}\frac{\varphi_3}{r}\right)\right] \tag{25c}$$

$$K_{22}=A_e\left[C_1r\left(C_{32}D_1+C_{33}C_1\right)+D_1r\left(C_{22}D_1+C_{23}C_1\right)\right] \tag{25d}$$

$$K_{24}=A_e\left[C_1r\left(C_{32}D_2+C_{33}C_2\right)+D_1r\left(C_{22}D_2+C_{23}C_2\right)\right] \tag{25e}$$

$$K_{26}=A_e\left[C_1r\left(C_{32}D_3+C_{33}C_3\right)+D_1r\left(C_{22}D_3+C_{23}C_3\right)\right] \tag{25f}$$

The other elements for *j*=1, 2, 3 and *i*=2, 3 in Eqs. (15) and (21) have been obtained in the similar state which result the element stiffness matrix finally.

The only external stress on the boundary of cylinder with constant thickness under internal pressure is $|\sigma_r|=p$, means that τ_{rz} and σ_z are equal to zero. Therefore, in expanded equations, the right side of indicial Eq. (20) is equal to zero.

Considering the triangular element, as shown in Fig. 3, the only component of stress for all elements which 1-3 lines are on the inner radius ($r=r_{in}$) is $|\sigma_r|=p$. Therefore, the only term of force for these elements in three equations resulted from indicial Eq. (15) is $\int_c r\phi_i\sigma_r dz$.

© 2015 IAU, Arak Branch

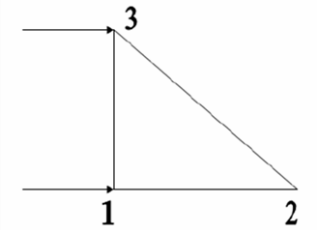

Fig.3
Sample of triangular element under loading.

In these elements, we have:

$$\sigma_r = \sigma_{r_i}\,\phi_1 + \sigma_{r_3}\,\phi_3 = p\left(\phi_1 + \phi_3\right) \tag{26}$$

Therefore, the force vector have been conducted as follow:

$$F_{r_i} = p r_i \int \phi_i \left(\phi_1 + \phi_3\right) dz \tag{27}$$

On the other hand, we have:

$$\begin{cases} \int_1^3 \phi_1^2 \; dz = \dfrac{1}{3}\, l_{13} \\ \int_1^3 \phi_3^2 \; dz = \dfrac{1}{3}\, l_{13} \\ \int_1^3 \phi_1\, \phi_3 \; dz = \dfrac{1}{6}\, l_{13} \end{cases} \tag{28}$$

where l_{13} is the length correspond to 1-3 line of element. Therefore, the force vector components of the elements with 1-3 lines on inner radius are:

$$F_r = \begin{Bmatrix} \dfrac{p r_1}{2}\left(z_3 - z_1\right) \\ 0 \\ \dfrac{p r_3}{2}\left(z_3 - z_1\right) \end{Bmatrix} \tag{29a}$$

$$F_z = \begin{Bmatrix} 0 \\ 0 \\ 0 \end{Bmatrix} \tag{29b}$$

where $r_1 = r_3 = r_{in}$.

Finally, the matrices form of six independent equations for these elements have been obtained:

$$\begin{bmatrix} k_{11} & k_{12} & k_{13} & k_{14} & k_{15} & k_{16} \\ k_{21} & k_{22} & k_{23} & k_{24} & k_{25} & k_{26} \\ k_{31} & k_{32} & k_{33} & k_{34} & k_{35} & k_{36} \\ k_{41} & k_{42} & k_{43} & k_{44} & k_{45} & k_{46} \\ k_{51} & k_{52} & k_{53} & k_{54} & k_{55} & k_{56} \\ k_{61} & k_{62} & k_{63} & k_{64} & k_{65} & k_{66} \end{bmatrix} \begin{Bmatrix} a_1 \\ b_1 \\ a_2 \\ b_2 \\ a_3 \\ b_3 \end{Bmatrix} = \begin{Bmatrix} F_{r_1} \\ F_{z_1} \\ F_{r_2} \\ F_{z_2} \\ F_{r_3} \\ F_{z_3} \end{Bmatrix} \tag{30}$$

For other elements outside the boundary, the components of force vector (the right side of matrices form of Eq. (30)) are equal to zero. The numerical solution is carried out by writing the program in MAPLE 16.

© 2015 IAU, Arak Branch

3 NUMERICAL ANALYSIS OF PRESSURE VESSEL

In order to prove the validity of the current solution for analyzing a FG cylinder, a numerical simulation has been investigated. The ANSYS 13 package was used in the static analysis of thick hollow cylinder with constant thickness. The internal pressure of the vessel is assumed to be constant with the value of $p = 100\,\text{MPa}$.

As a case study, a thick cylinder whose elasticity modulus varies along longitudinal direction has been considered by the following characteristics: $r_i = 15\,\text{cm}$, $L = 60\,\text{cm}$ and $t = 4\,\text{cm}$. The numerical and analytical results have been investigated for clamped-free boundary conditions.

The basic elastic modulus is supposed to be $E_0 = 200\,\text{GPa}$. The value of Poisson's ratio is $\upsilon = 0.3$. In ANSYS simulation, the vessel along the longitudinal direction divided to 100 equal and joined layers by the assumption of inhomogeneity constant equal to $\beta = 2$. The PLANE82 element in axisymmetric mode, which is an element with eight nodes and two translational degrees of freedom in the axial and radial directions per each node, was used for discretion.

4 RESULTS AND DISCUSSION

In Figs. 4 and 5, the radial and axial displacement distribution at middle layer of the cylinder resulted from semi analytical and numerical solution has been shown for $\beta = 2$. The radial displacement increases around the clamped boundary while by increasing the length in the next parts of the vessel, the radial displacement decreases. The absolute value of axial displacement increases along the longitudinal direction. Considering shear stresses, the layers around the clamped boundary have been affected by clamped conditions and show different behavior in comparison with next parts of vessel.

Figs. 6 - 10 show the distribution of radial, circumferential, axial, shear and von Mises stresses at middle layer of the vessel with the findings of both semi analytical solution and finite element method (FEM). Comparison of the results shows appropriate agreement between two methods. It is obviously apparent that stresses at points near the boundaries are different from the other areas under the effect of shear stresses resulted from clamped boundary condition. At points away from the boundaries, stresses does not show significant variations along the longitudinal direction, while at points near the boundaries, the reverse holds true.

Because of compression along the radial direction, the radial stress at the middle layer of vessel is nearly negative (Fig. 6). Fig. 7 shows that the circumferential stress is also negative. Furthermore, the axial stress approximately from the half of the vessel close to the free end has the value of zero (Fig. 8). It is obviously observed from Fig. 9 that there are shear stresses near the clamped ends of the cylinder. The shear stresses at points away from the clamped boundary at different layers are zero while at points near the boundaries, the shear stresses are significant. Clamped b.c. cause axial and shear stresses at the layers closed to the clamped end of the vessel. It is obviously observed in Fig. 10 that the von Mises stress at the middle layer of vessel is positive.

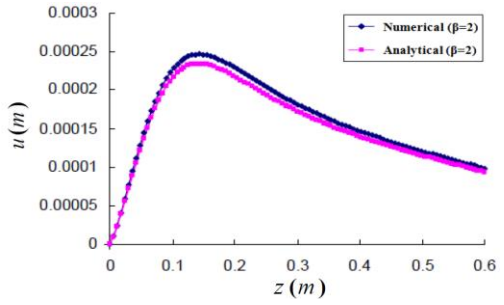

Fig.4
Distribution of radial displacement at middle of the vessel for $\beta = 2$.

© 2015 IAU, Arak Branch

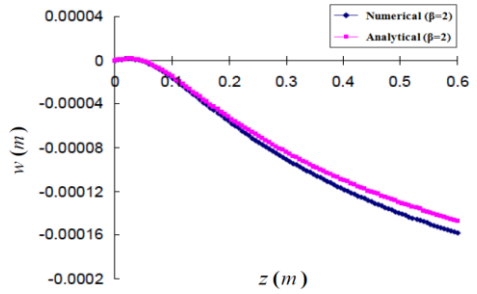

Fig.5
Distribution of axial displacement at middle of the vessel for $\beta = 2$.

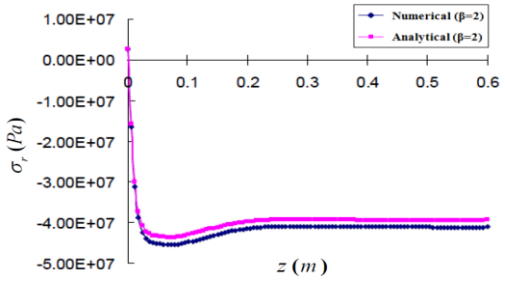

Fig.6
Distribution of radial stress at middle of the vessel for $\beta = 2$.

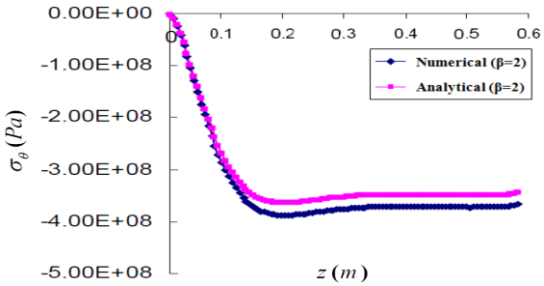

Fig.7
Distribution of circumferential stress at middle of the vessel for $\beta = 2$.

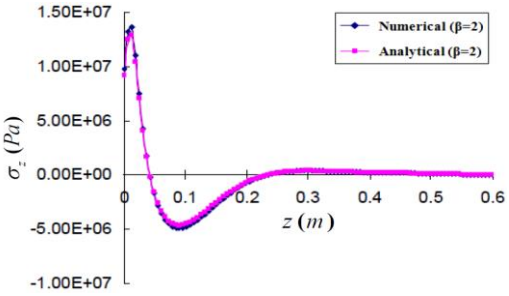

Fig.8
Distribution of axial stress at middle of the vessel for $\beta = 2$.

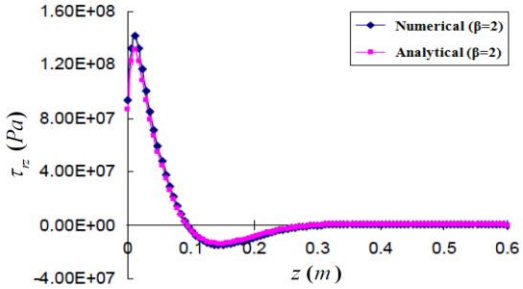

Fig.9
Distribution of shear stress at middle of the vessel for $\beta = 2$.

© 2015 IAU, Arak Branch

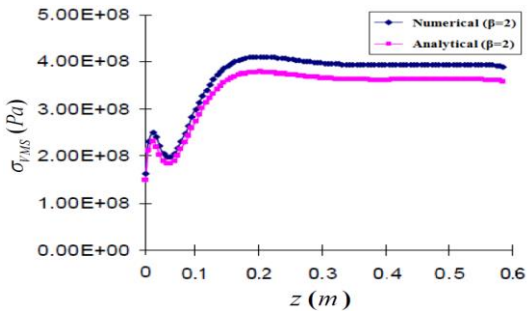

Fig.10
Distribution of von Mises stress at middle of the vessel for $\beta = 2$.

In order to investigate the inhomogeneity constant effect on displacements and stresses of FGM cylindrical pressure vessels with exponential variation of elastic modulus along the longitudinal direction, the value of inhomogeneity constant is supposed to vary in the range of 2 and -2. In order to normalize the parameters, the values of displacements and stresses have been divided on thickness and internal pressure of the vessel, respectively.

$$U^* = u/t, W^* = w/t, \sigma_r^* = \sigma_r/p, \sigma_\theta^* = \sigma_\theta/p, \sigma_z^* = \sigma_z/p, \tau_{rz}^* = \tau_{rz}/p, \sigma_{VMS}^* = \sigma_{VMS}/p \tag{31}$$

The normalized radial and axial displacement distribution along the longitudinal direction at internal and middle surfaces of the pressure vessel for different inhomogeneity constants have been shown in Figs. 11-14.

As depicted in Figs. 11 and 12, the radial displacement of vessels for negative inhomogeneity constants have increased along the longitudinal direction. For positive inhomogeneity constants, increasing the height from 0.2 to end of the vessel causes a decrease in the radial displacement. By increasing the inhomogeneity constants, the slope of radial displacement variations would increase.

It is observed from Fig. 13 that the normalized absolute value of axial displacement for negative values of β is higher than homogenous materials. The axial displacement of layers close to the clamped end is positive while along the longitudinal direction from clamped end to free one, the value of axial displacement is negative. FGM pressure vessels with positive values of β shows the same behavior from the viewpoint of the absolute value of axial displacement as the vessels with negative values of β . Fig. 14 shows that decreasing inhomogeneity constants from positive values to the negative one in range of $-2 \le \beta \le 2$ causes higher values of the axial displacement. As a result, the greatest displacements occur at the free end of vessel. Furthermore, pressure vessels with positive values of β have less displacement than negative ones.

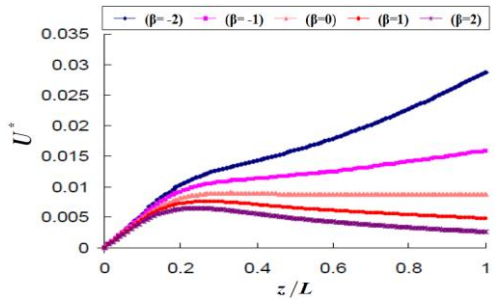

Fig.11
Radial displacement distribution at internal surface of the vessel.

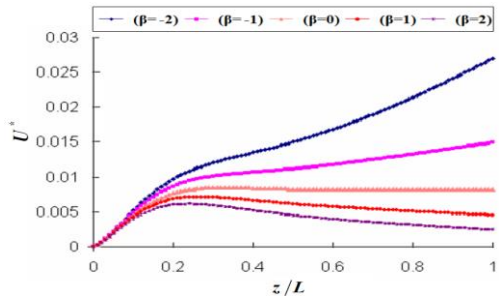

Fig.12
Radial displacement distribution at middle surface of the vessel.

© 2015 IAU, Arak Branch

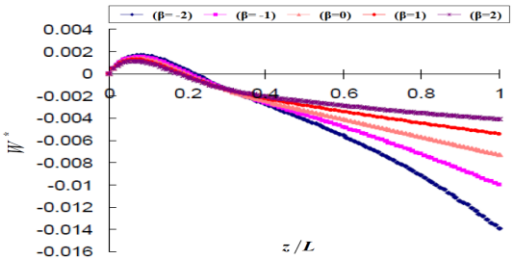

Fig.13
Axial displacement distribution at internal surface of the vessel.

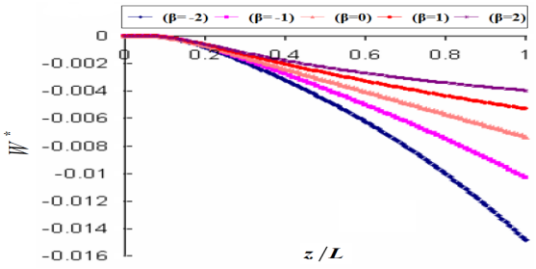

Fig.14
Axial displacement distribution at middle surface of the vessel.

Figs. 15-23 show the normalized stresses consist of radial, circumferential, axial, shear and von Mises stress along the axial at the internal and middle layers of the vessel for different inhomogeneity constants, respectively. Investigating the stress graphs at the inner and middle layers of pressure vessels improve that the radial and circumferential stresses at the points away from the clamped end are constant means that they are independent from the longitudinal direction. Furthermore, the radial stress at the external layer is zero (traction free surface) while its absolute value increase toward the internal layer. The shear and axial stresses at the points far from clamped boundary of the cylinder are equal to zero which satisfy plane elasticity theory. The layers near the clamped end have nonzero values of shear and axial stresses under the effect of clamped boundary conditions. The maximum stress at the thickness of vessel occurs for $\beta = -2$, whereas the minimum one has been observed in case of $\beta = 2$. As a result, decreasing inhomogeneity constant of the vessel from the positive values to the negative ones in range of $-2 \le \beta \le 2$ causes an increase in maximum stress of the vessel.

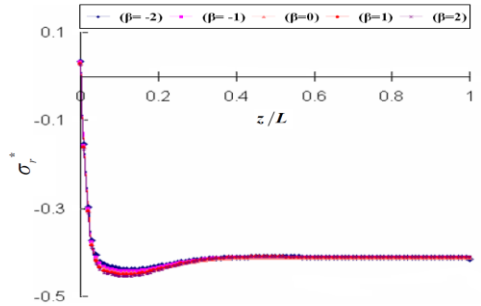

Fig.15
Radial stress distribution at middle surface of the vessel.

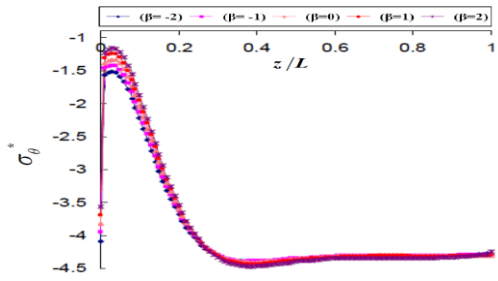

Fig.16
Circumferential stress distribution at internal surface of the vessel.

© 2015 IAU, Arak Branch

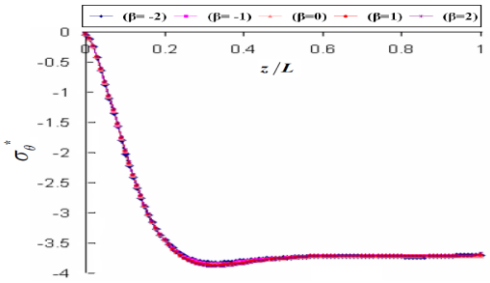

Fig.17
Circumferential stress distribution at middle surface of the vessel.

Furthermore, investigating Figs. 11-23 show that the longitudinal variation of elastic modulus has been mainly affected only by the radial and axial displacements of pressure vessels while its effect on the values of stresses is too small.

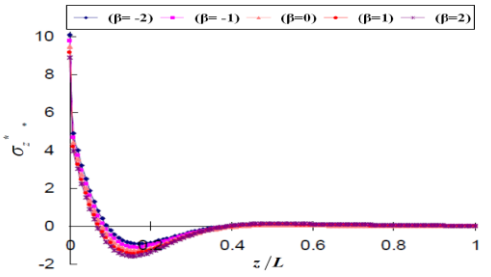

Fig.18
Axial stress distribution at internal surface of the vessel.

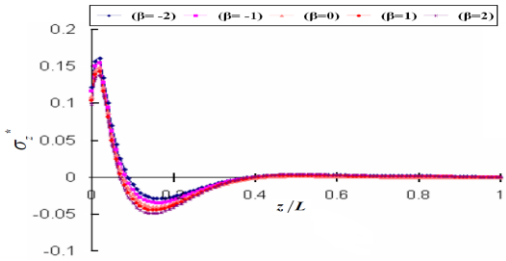

Fig.19
Axial stress distribution at middle surface of the vessel.

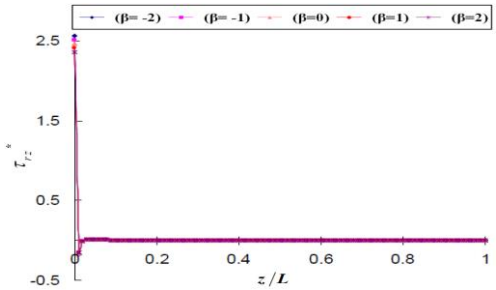

Fig.20
Shear stress distribution at internal surface of the vessel.

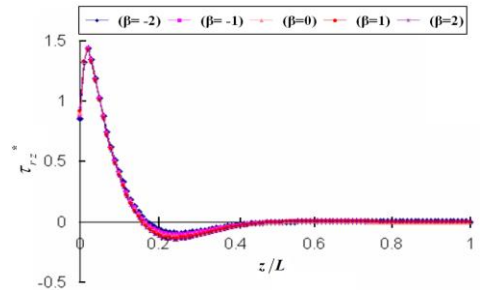

Fig.21
Shear stress distribution at middle surface of the vessel.

© 2015 IAU, Arak Branch

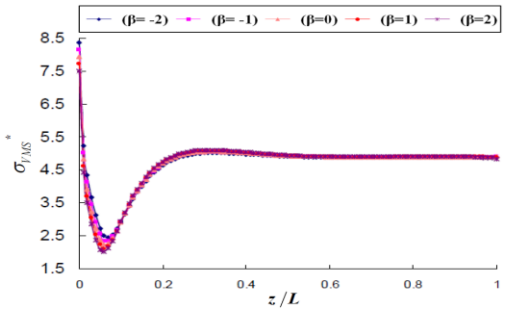

Fig.22
Von Mises stress distribution at internal surface of the vessel.

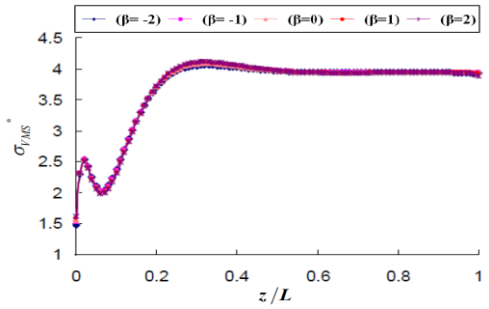

Fig.23
Von Mises stress distribution at middle surface of the vessel.

5 CONCLUSIONS

The results obtained from the analysis of FGM thick-walled cylindrical pressure vessel with exponential variation of elastic modulus along the longitudinal direction under internal pressure in clamped-free ends condition indicate that: The longitudinal variations of elastic modulus affect mainly on the radial and axial displacements distribution of cylindrical pressure vessel while its effect on the stress values is too small. For negative inhomogeneity constants in range of $-2 \le \beta \le 2$, the radial displacement values of pressure vessel increase along the longitudinal direction from the clamped end to the free one while for positive ones in the same range, they will decrease from 0.2 of height. Increasing inhomogeneity constant in range of $-2 \le \beta \le 2$ accelerate the variations of radial displacement. Thus, the maximum radial displacement of vessel occurs for $\beta = -2$. Decreasing the inhomogeneity constant from positive values to negative ones in range of $-2 \le \beta \le 2$ will cause an increase in the axial displacement of vessel along the longitudinal direction. Therefore, the maximum axial displacement of vessel occurs for $\beta = -2$. As a result, the greatest displacements occur at the free end of vessel. Furthermore, pressure vessels with positive values of β have less displacement than the negative ones. The radial and circumferential stresses at points away from boundary of the vessel are constant means that they are independent from the longitudinal direction. There are shear and axial stresses near clamped end of the cylinder. Shear and axial stresses at points away from the clamped end at different layers of the cylinder are equal to zero which satisfy plane elasticity theory. However, at points near z=0, the mentioned stresses are significant under the effect of clamped boundary conditions. By decreasing the inhomogeneity constant of vessel from positive values to negative ones in range of $-2 \le \beta \le 2$, the maximum stress of vessel will increase. It can be concluded that existence of shear stresses causes variation of stresses through the longitudinal direction near the clamped end of vessel, while zero values of shear stresses at the points far away from the clamped ends causes the corresponding stresses to be constant through the longitudinal direction.

ACKNOWLEDGMENTS

The authors would like to acknowledge Shahrood University, Shahrood, Iran for financial support of this article under a scientific and technical research project.

© 2015 IAU, Arak Branch

REFERENCES

[1] Fukui Y., Yamanaka N., 1992, Elastic analysis for thick-walled tubes of functionally graded materials subjected to internal pressure, *JSME International Journal Series I* **35**(4): 891-900.

[2] Tutuncu N., Ozturk M., 2001, Exact solution for stresses in functionally graded pressure vessel, *Composites Part B: Engineering* **32**: 683-686.

[3] Jabbari M., Sohrab pour S., Eslami M.R., 2002, Mechanical and thermal stresses in a functionally graded hollow cylinder due to radially symmetric loads, *International Journal of Pressure Vessel and Piping* **79**: 493-497.

[4] Eipakchi H.R., Khadem S.E., Rahimi G.H., 2008, Axisymmetric stress analysis of a thick conical shell with varying thickness under nonuniform internal pressure, *Journal of Engineering Mechanics* **134**: 601-610.

[5] Eslami M.R., Babaei M.H., Poultangari R., 2005, Thermal and mechanical stresses in a functionally graded thick sphere, *International Journal of Pressure Vessel and Piping* **82**: 522-527.

[6] Dai H.L., Fu Y.M., Dong Z.M., 2006, Exact solutions for functionally graded pressure vessels in a uniform magnetic field, *International Journal of Solids and Structures* **43**: 5570-5580.

[7] Naghdabadi R., Kordkheili S.A., 2005, A finite element formulation for analysis of functionally graded plates and shells, *ASME Journal of Applied Mechanics* **74**: 375-386.

[8] Hongjun X., Zhifei S., Taotao Z., 2006, Elastic analyses of heterogeneous hollow cylinders, *Mechanics Research Communications* **33**(5): 681-691.

[9] Zhifei S., Taotao Z., Hongjun X., 2007, Exact solutions of heterogeneous elastic hollow cylinders, *Composite Structures* **79**: 140-147.

[10] Tutuncu N., 2007, Stresses in thick-walled FGM cylinders with exponentially-varying properties, *Engineering Structures* **29**: 2032-2035.

[11] Ghannad M., Nejad M.Z., 2010, Elastic analysis of pressurized thick hollow cylindrical shells with clamped-clamped ends, *Mechanika* **5**(85): 11-18.

[12] Ghannad M., Rahimi G.H., Zamani Nejad M., 2012, Determination of displacements and stresses in pressurized thick cylindrical shells with variable thickness using perturbation technique, *Mechanika* **18**(1): 14-21.

[13] Gharooni H., Ghannad M., 2012, Analytical solution of rotary pressurized FGM cylinder by the usage of first order shear deformation theory, *11th Conference of Iranian Aerospace Society* **15024**: 195.

[14] Liu L., Li J., Ding M., Yang X., 2007, Development of SiC/(W, Ti)C gradient ceramic nozzle materials for sand blasting surface treatments, *International Journal of Refractory Metals and Hard Materials* **25**(2): 130-137.

[15] Liu L., Deng J., 2008, Study on erosion wear mechanism of SiC/(W,Ti)C gradient ceramic nozzle material, *Journal of Key Engineering Materials* **375**(376): 440-444.

[16] Asemi K., Salehi M., Akhlaghi M., 2011, Elastic solution of a two-dimensional functionally graded thick truncated cone with finite length under hydrostatic combined loads, *Acta Mechanica* **217**(1-2): 119-134.

[17] Masoud Asgari M., Akhlaghi M., 2010, Transient thermal stresses in two-dimensional functionally graded thick hollow cylinder with finite length, *Archive of Applied Mechanics* **80**(4): 353-376.

[18] Ghannad M., Rahimi G.H., Zamani Nejad M., 2013, Elastic analysis of pressurized thick cylindrical shells with variable thickness made of functionally graded materials, *Composites: Part B* **45**: 388-396.

© 2015 IAU, Arak Branch